



Evolution of the nanostructure of Pt and Pt–Co polymer electrolyte membrane fuel cell electrocatalysts at successive degradation stages probed by X-ray photoemission

Mushtaq Ali ^{a, b, *}, Agnieszka Witkowska ^{c, **}, Mamatimin Abbas ^d, Roberto Gunnella ^b, Andrea Di Cicco ^b

^a Department of Physics, CIIT, Islamabad, Pakistan

^b CNISM, Physics Division, School of Science and Technology, University of Camerino, Italy

^c Department of Solid State Physics, Gdańsk University of Technology, Poland

^d Laboratoire IMS, UMR 5218 CNRS, ENSCBP, France



HIGHLIGHTS

- Structural changes in aged Pt/C and PtCo/C catalysts worked in PEMFC were studied.
- Detailed XPS analysis was applied to extend previous TEM/XRD/XAFS observations.
- Aged Pt/C: large particles are formed mainly in cathode/membrane interface region.
- Aged PtCo/C: stable nanoparticles with Pt₄Co core covered by Pt-skin are formed.
- Pt-skin formation is the main factor responsible for mild variation in PtCo/C activity.

ARTICLE INFO

Article history:

Received 8 June 2014

Received in revised form

21 July 2014

Accepted 7 August 2014

Available online 14 August 2014

Keywords:

PEMFC

Pt-based cathode catalysts

Aging

Nanostructure

XPS

ABSTRACT

We present a set of XPS (X-ray photoemission spectroscopy) measurements and detailed data-analysis of electrodes for polymer electrolyte membrane fuel cell (PEMFC) based on carbon supported catalysts (Pt and Pt–Co) subjected to a step-like potential cycling (accelerated degradation test). The results of the measurements complete and corroborate parallel TEM (transmission electron microscopy), XRD (X-ray diffraction) and XAS (X-ray absorption spectroscopy) results pointing at a modification of the nanostructure of the catalyst grains. The surface sensitivity of the XPS measurements is used to study the modification of the reactive surface structure of the nanoparticles and the interplay of reactivity and dissolution/precipitation/agglomeration of metal clusters during the catalyst work. The combination of XPS results with XRD, XAS and TEM ones allowed us to obtain a model for the structural changes in Pt–Co nanoparticles occurring during operation. The main structural modifications, in which predominantly Co atoms are involved, occur during the first hours of catalyst operation changing the stoichiometry and degree of disorder in external particles shell. In the last stages of the degradation process, core–shell particles structure, with ordered Pt₄Co core and Pt-rich shell (and finally Pt-skin), is formed possibly explaining higher Pt–Co catalyst stability (structural and electrochemical) than pure Pt catalyst.

© 2014 Elsevier B.V. All rights reserved.

1. Introduction

The development of new materials that can solve challenging problems in the areas of clean energy production, conversion and

storage is of paramount importance in the quest to find an alternative to environmentally unfriendly fossil-fuel use. One promising alternative is the polymer electrolyte membrane fuel cell (PEMFC) [1–6]. However, to make hydrogen based energy systems a vibrant and competitive force, many problems still need to be solved [7]. The main one is to find a more stable, effective and less expensive catalyst than Pt for the oxygen-reduction reaction (ORR).

One of the possible ways to create electro-catalysts with unique properties is to form alloy of two or more metals. Several investigations [8–13] have been carried out in the Pt-based alloys to

* Corresponding author. Department of Physics, CIIT, Islamabad, Pakistan.

** Corresponding author.

E-mail addresses: mushtaqali@comsats.edu.pk (M. Ali), agnieszka@mif.pg.gda.pl (A. Witkowska).

determine the role of alloying on the electro-catalytic activity of Pt for the ORR. However, definitive determination still remains elusive. One of the difficulties in determining the effect of alloying in supported catalysts is that the catalyst activity strongly depends on the microstructure and/or on the method of preparation. Therefore, the effects of chemical composition, atomic surface structure and surface segregation-induced electronic properties change on the supported bimetallic nanoparticles reactivity are still discussed. Moreover, the particles of alloyed Pt usually have not either the same size or shape as the pure Pt reference catalysts and a simple comparison of activity normalized either by mass or surface area is insufficient to identify a true alloying effect. This complexity emphasizes the need to use well characterized materials to identify the fundamental mechanisms of the ORR and of the catalyst durability.

Recently, Co containing Pt alloys attracted large interest in their applications in fuel cell technology, especially as a cathode catalyst in PEMFC. Many works (e.g. Refs. [14–19]) were devoted to fine analysis of the nanoalloys structure and possible correlations between structure and morphology and functional properties. There is a consensus that Pt–Co alloys offer a favorable intrinsic enhancement in electrocatalytic activity and stability [16–18]. In this work we focus on the changes induced by real fuel cell working conditions observed by X-ray photoelectron spectroscopy (XPS) in simple commercial Pt and bimetallic Pt–Co nanocatalysts supported on Vulcan (E-TEK). The atomic level structure of considered nanomaterials (in the powder form and in the form of thin catalytic layer being a part of working PEMFC) was the subject of our previously published papers [18–22], where a detailed characterization (accounting for size effects and chemical disorder) was performed by transmission electron microscopy (TEM), X-ray diffraction (XRD) and X-ray absorption spectroscopy (XAS). Combination of these methods resulted in a very precise description of nanocatalysts structure (i.e. nanoparticles morphology and their size distributions, geometric structure on the atomic level by mean of pair and angle distribution functions) and gave possibility to observe subtle structural changes induced by PEMFC working conditions (temperature, cell potential, time). Despite that such techniques are in general bulk-sensitive and give information about mean short- and medium-range structure. Combining them we have been able to extract some information about nanoparticles surface structure (so important from the catalytic point of view). We have noted their modifications as a result of various applied FC working conditions and possible core–shell structure formation in Pt–Co nanocatalyst. However, direct and detailed study using surface sensitive technique was needed to confirm our preliminary results. For this reason, we used XPS technique to investigate the FC working time-dependent changes in the atomic composition and in the oxidation states of the Pt and Co atoms belonging to the nanoparticles surface.

The paper is organized as follows: after the section containing experimental details, the results of XPS data analysis of Pt and Pt–Co-based electrodes are presented in Section 3. Section 4 is dedicated to the discussion of the obtained results. Section 5 contains the main conclusions of this work.

2. Experimental

2.1. Sample preparation

XPS measurements were performed on two pristine powders 20%Pt/Vulcan (E-TEK, hereafter called Pt/C) and 30%PtCo/Vulcan (E-TEK, hereafter called PtCo/C) and on electrodes prepared on the basis of these powders. To prepare the electrodes the required quantity of metal/Vulcan catalytic powder (Pt/C or PtCo/C) was

placed in a closed glass vial with isopropyl alcohol and 5% Nafion solution (Nafion content was 35% wt.). The suspension, stirred at room temperature for 24 h, was then brushed on the gas diffusion layer (ELAT GDL, LT1200W, from E-TEK) and dried at 80 °C for 30 min. The total metal loading was computed from the weight and for all Pt/C and PtCo/C electrodes was about 0.9 and 1.5 mg cm⁻², respectively. Such electrodes were used as cathodes in membrane electrode assemblies (MEAs). Moreover, MEAs were composed of Nafion N-112R (DuPont) as a polymer electrolyte and a Pt standard electrode on the anode side (E-TEK, Pt loading 0.5 mg cm⁻²). MEAs (not hot pressed in this case to facilitate their dismantling to perform structural analysis of the catalysts) were then placed into a single fuel cell (FC) and conditioned in H₂/O₂ flows on the anode/cathode side, respectively, at 70 °C and 0.6 V for 2–4 h. After that the degradation process of electrocatalyst was performed by using an accelerated-test methodology based on the step-like potential cycling, i.e. FC was worked 1 h at 0.6 V and 1 h at open circuit voltage (OCV). The total working time amounted to 150 h (the time taken for conditioning did not count toward the working time). For both type of electrocatalysts the following set of samples was prepared:

1. pp-Pt/C – pristine powder; 0-Pt/C – as prepared electrode; 100-Pt/C and 150-Pt/C – cathode worked for 100 h and 150 h, respectively.
2. pp-PtCo/C – pristine powder; 0-PtCo/C – as prepared electrode; 50-PtCo/C, 100-PtCo/C and 150-PtCo/C – cathode worked for 50 h, 100 h and 150 h, respectively.

After each degradation stage the electrochemical performance of the single FC was checked (see Section 2.2) and then cell was dismantled and cathode catalyst was subjected to *ex situ* XPS measurements (see Section 2.3).

2.2. Electrochemical performance of single FC

In Fig. 1 comparison between considered cathode catalysts activity defined by FC current density measured at 0.8 V at the end of

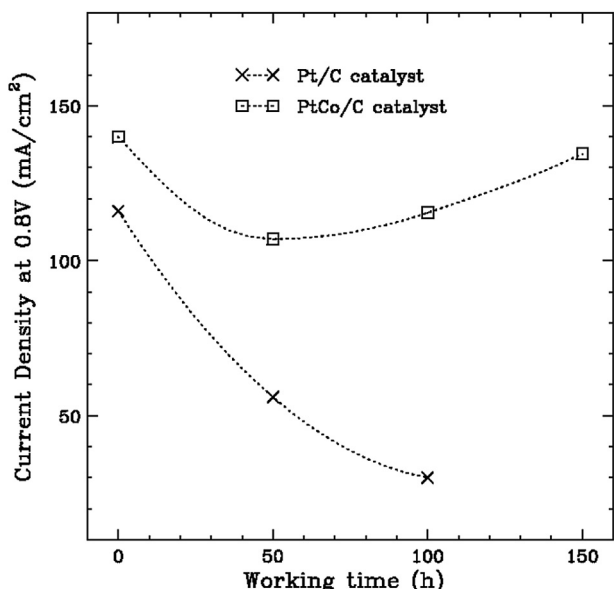


Fig. 1. Pt/C and PtCo/C cathode catalyst activity (defined by FC current density at 0.8 V) as a function of fuel cell working time (dotted curves are only an eye guide). Detailed information about FC working conditions can be found in the text.

each degradation stage is presented. The following working conditions were applied during conditioning and accelerated degradation test, and then during the FC performance check: H_2 flux = 100 ml min⁻¹, O_2 flux = 200 ml min⁻¹, $T(\text{cell}/H_2/O_2)$ = 70/70/70 °C, $p(O_2) = p(H_2)$ = 1 bar for Pt/C catalyst and 2 bar for PtCo/C catalyst.

From Fig. 1 it is easy to note a significant difference between Pt/C and PtCo/C cathode catalyst activity and their variation as a function of FC working time. In the case of Pt/C electrocatalyst 100 h of work under step-like potential cycling conditions was enough to lose over 75% of initial current density. Degradation prolonged by subsequent 50 h led to the complete fuel cell deactivation (polarization curve was not collected). Whereas, in the case of PtCo/C electrocatalyst 150 h of work under the same conditions did not strongly affect the cathode activity. However, it should be underlined a slight drop of current density occurred during the first 50 h of work and then their progressive increase. Other details as regards electrochemical performance of FC, particularly when the cathode activation region is considered, can be found in Ref. [19].

Despite these differences, previously obtained XRD/TEM/XAS results led us to the following general conclusions, valid for both type of catalysts: 1) changes in the mean structural and chemical order in the Pt and Co atoms local environment did not affect the FC performance; 2) electrochemical parameters of FC depended predominantly on the metallic phase structure at nano- and microscopic level and on the nanoparticle size distribution instability. However, some important issues as the high stability of Pt–Co nanoparticle size distribution and the mild variation in PtCo/C cathode catalyst activity during FC operation are still unexplained.

2.3. XPS measurements and analysis

The X-ray photoelectron spectra of the samples were recorded with a concentric hemispherical analyzer (CHA) in ultra high vacuum (UHV) with a base pressure below 10^{-9} Torr by employing Al-K α unmonochromatised source (1486.7 eV) operating at 10 kV and a constant pass energy of 58.5 eV for survey scans, as well as for detailed scans. All binding energy values were charge-corrected to the adventitious C(1s) signal which was set at 285.1 eV. The quantitative evaluation of each peak was obtained by dividing the integrated peak area (PA) by atomic sensitivity factor (ASF(Pt_{4f}) = 4.4, ASF(Co_{2p3/2}) = 2.5, ASF(C_{1s}) = 0.25) [23] after subtracting background [24,25].

Atomic concentration and the relative amounts of metallic and oxide components of Pt and Co were calculated from Pt(4f) and Co(2p_{3/2}) signals, respectively. Thus, the Pt(4f) spectra were deconvoluted into three separate doublets (4f_{7/2}, 4f_{5/2}) of valency, respectively: metallic platinum → Pt⁰ (71.66, 75.01 eV), Pt(OH)₂/PtO → Pt^{II} (73.06, 76.41 eV) and PtO₂ → Pt^{IV} (74.65, 77.9 eV). The spin-orbit splitting of the doublets and the energy shift of the Pt metallic with respect to Pt^{II} and Pt^{IV} were similar to the values reported in the references [23,26,27]. During the fitting, constant width and shape for the doublet peaks of Pt⁰, Pt^{II} and Pt^{IV} were used for all the samples. The branching ratio was kept at the statistical value. At the same time, the Co(2p_{3/2}) spectra obtained for 30%PtCo/Vulcan electrocatalyst were fitted to estimate the relative amounts of various Co components. The energy shift of the Co⁰ to Co^{II} has been precisely determined from the Co oxidized foil (obtained value was comparable to the values found in Refs. [23,28]). The satellite structure associated with the Co(2p) line of Co^{II} is quite complex because of the two strong components at 2.1 eV and 5.8 eV above the principal line of Co^{II} [28]. Therefore, the Co(2p_{3/2}) spectra were deconvoluted into four peaks corresponding to the metallic cobalt → Co⁰ (778.25 eV), CoO → Co^{II} (780.25 eV) and to two shake-up satellite peaks of Co^{II} (782.35 eV and 786.05 eV). In this

case the following constraints were used: equal width and shape for Co⁰, Co^{II} and two shake-up satellite peaks. The intensity ratios of Co^{II} to shake-up₁ and shake-up₂ were considered as free parameters.

3. Results

Fig. 2 reports survey spectra of the Pt/C and PtCo/C electrocatalysts in which all the elements found by chemical analysis in the powder and electrodes can be distinguished, i.e. peaks which correspond to Pt, Co, C, and O elements and F(1s) strong signal present in spectra of as prepared and used (degraded) electrodes indicating the presence of Nafion (ionomer phase) in the catalytic layer. The Pt/Co atomic relation in pristine powder and in the electrodes obtained by normalization of Co signal are shown in Table 1. For comparison the results of XRD- and XAS-extracted Pt/Co ratio [19] are also presented in Table 1. Other parameters obtained during the previous structural analysis of considered samples (like particle mean diameter and chemical order parameter), useful for subsequent discussion, are also shown in the table.

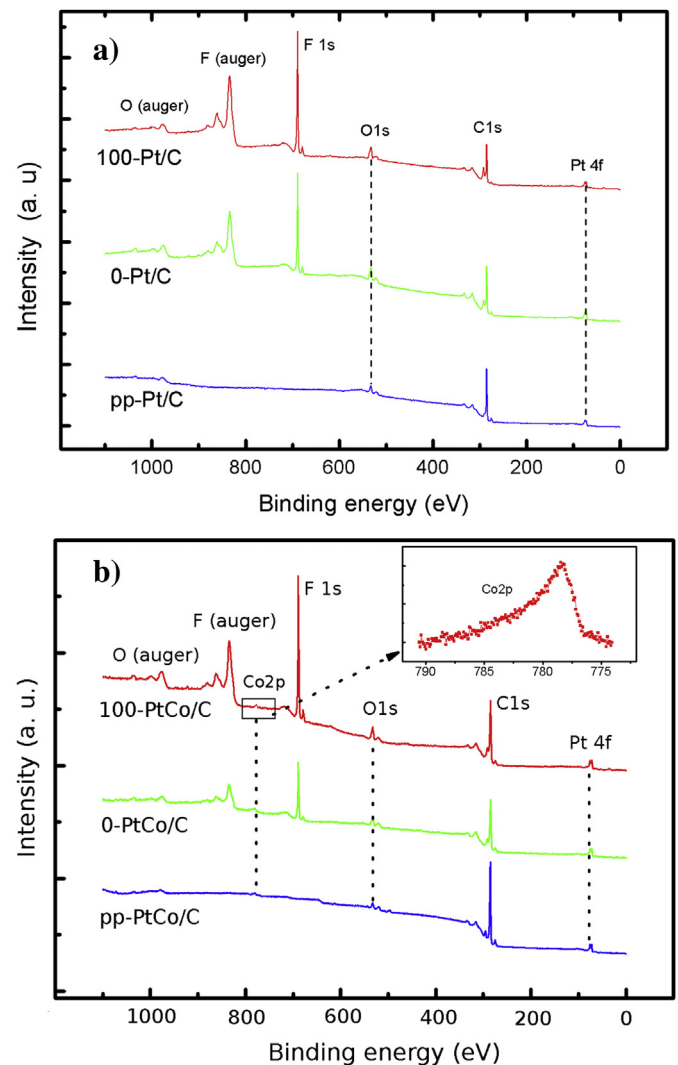


Fig. 2. The survey XPS scan recorded for: a) 20%Pt/Vulcan and b) 30%PtCo/Vulcan electro-catalysts in the pristine powder forms (pp-Pt/C, pp-PtCo/C), as prepared electrodes (0-Pt/C, 0-PtCo/C) and electrodes worked for 100 h (100-Pt/C, 100-PtCo/C).

Table 1

XPS-extracted Pt/Co atomic ratio in 30%PtCo/Vulcan samples. Pt/Co relations obtained for considered samples by XRD and XAS analysis [19] are also shown for comparison. Other parameters presented: D_{ave} – particles mean diameter as extracted from XRD and TEM data [19,22] (I, II indices – mean value of the first and second peak, respectively, in “bimodal” particles size distribution profile), s – chemical order parameter for a bimetallic alloy (define in Ref. [18], $s = 1$ indicates perfect chemical order) and calculated on the base of XAFS data [19].

Sample	Pt/Co atomic ratio			D_{ave} [nm]		s
	XPS	XRD	XAS	XRD	TEM	
pp-PtCo/C	4.4(2)	3.08(2)	2.65(2)	4.3(9)	5.5(5)	0.6(1)
0-PtCo/C	3.7(2)	3.5(1)	2.65(4)	5.0(5)	5.4(5)	0.5(1)
50-PtCo/C	4.4(2)	4.0(5)	3.8(1)	4.9(5)	5.3(5)	0.8(1)
100-PtCo/C	4.6(2)	—	—	—	—	—
150-PtCo/C	4.9(2)	4.0(5)	3.9(1)	5.0(5)	5.4(5)	0.8(1)
pp-Pt/C				2.5(3)	2.40(5)	
0-Pt/C				2.4(1)	1.95(3)	
100-Pt/C				2.7(1)	2.30(3) ^I	
150-Pt/C					4.55(3) ^{II}	
				3.1(2)	2.75(3) ^I	
					6.36(3) ^{II}	

On the basis of XPS measurements it is also possible to estimate the relative valency of Pt and Co components present on the external shell of nanoparticles in the considered electrocatalysts. Fig. 3 shows XPS Pt(4f) (panels a and b) and Co(2p_{3/2}) (panel c) spectra and their components for pristine powders (pp-Pt/C and pp-PtCo/C), as prepared (0-Pt/C and 0-PtCo/C) and aged (100-Pt/C and 50-PtCo/C) electrodes. The relative amounts of metallic Pt⁰ and its oxides determined from the best fit of Pt(4f) spectra for all samples are shown in Table 2. Whereas, relative amounts of Co⁰ and Co^{II} obtained from the best fit of Co(2p_{3/2}) spectra for all samples are shown in Table 3.

4. Discussion

At the first view the data presented in Table 1 revealed clear dependence on the catalyst particles nanostructure and FC working time. Moreover, differences in Pt/Co atomic ratio in each catalyst degradation stage as obtained by XPS, XRD and XAS techniques, having different sensitivity to the physical parameters, show the complexity of the structural changes occurred in the material during their operation. However, combining present XPS results with previous XRD, XAS and TEM ones, we constructed the model of the evolution of Pt and Pt–Co nanoparticles structure in PEMFC electrocatalysts in the subsequent degradation stages. Then, we used this model to discuss the data presented in Tables 2 and 3. In Section 4.1 the results related to pristine powders are considered. The nanoparticles structure in degraded PtCo/C and Pt/C electrodes is presented in Sections 4.2 and 4.3, respectively.

4.1. Pristine powders

Starting to consider data obtained for studied pristine powders, shown in Table 1, it should be underlined that: 1) because of the mean free path value of the considered photoelectrons (Pt(4f) and Co(2p_{3/2})), XPS measurements sampled at most 1-nm thick surface shell of metallic particles; 2) XRD-extracted value defines the stoichiometry of bulk crystalline phase and is insensitive on the presence of small particles or amorphous/disordered phase; 3) XAS-extracted Pt/Co atomic ratio is related to the ratio of the XAS spectra discontinuity at the Pt L₃ and Co K edges which are proportional to the total amount of each metal in the sample, including the Co not fully alloyed with Pt. In that way, the differences in Pt/Co atomic ratio value obtained by these techniques can indicate inhomogeneous Pt and Co atoms distribution in the sample. Table 1

shows that just such a case we had to deal with pp-PtCo/C catalyst. XPS spectra analysis gave the Pt:Co atomic relation equal to 4.4:1. At the same time, this ratio determined by XRD pattern and XAS spectra analysis clearly indicated a lower Pt content in the sample. Therefore, taking into account all these aspects and other data presented in Table 1, it can be established that pristine powder of considered Pt–Co alloy catalyst was composed of metallic nanoparticles with a mean diameter of about 5.5(5) nm (TEM-determined value, Table 1), having a core–shell structure. Pt–Co nanocrystalline core had a mean diameter of 4.3(9) nm and Pt₃Co stoichiometry (XRD-determined values, Table 1), whereas, chemically disordered shell exhibited larger Pt/Co atomic ratio, at least equal to 5.5 for an assumed shell thickness amounting to 0.5 nm (see also Fig. 4).

Comparing now data presented in Table 2 obtained for pristine powder of Pt/C and PtCo/C catalysts, first of all our attention is captured by the difference in relative amounts of oxidized Pt species (for pp-Pt/C catalyst total relative value is about 16% higher, Table 2). Due to different particles mean diameter and different particles surface composition direct comparison seems unjustified. However, taking into account the mean particle size in pristine powders (Table 1) and the structural model constructed above for pp-PtCo/C combining XRD/TEM/XAS and XPS data, it can be calculated that for pp-Pt/C about 50% of all platinum viewed by XPS measurement belongs to the nanoparticles surface, whereas in the case of pp-PtCo/C – only about 35%. This means that coverage of nanoparticle surface by Pt oxide species is lower for alloyed particles. Based on the obtained values and on the previous electrochemical tests (see e.g. Fig. 1), it can be observed that a lower mean surface Pt valency in pristine powder corresponds to a greater possible initial electrocatalyst activity and stability. Moreover, it can also be calculated that 25–30% of all Co atoms viewed by XPS measurement belongs to the particle surface in pp-PtCo/C sample. Whereas, the obtained during analysis a relative content of Co^{II} equaled 38(2)% (Table 3). This difference shows that small Co (or Co-rich alloy) particles and/or crystalline cobalt oxide are present in studied pristine material, consistent with previous TEM image analysis showing that about 5% of all particles in pristine powder had a diameter smaller than 2 nm [18].

4.2. Degraded PtCo/C electrocatalyst

Considering now electrocatalyst forming a cathode catalytic layer (having a total thickness of about 15–25 μm), it should be taken into account that in this case XPS measurement sampled external shell of metallic nanoparticles placed only close to the cathode/membrane interface (within about 1 nm, at the surface of the catalytic layer), where the catalyst was very intensively exploited in the oxygen reduction reaction. Whereas XRD and XAS measurements sampled the whole catalytic layer volume. Moreover, discussing the XPS data presented in Tables 2 and 3 it should be underlined that the measurements were performed *ex situ* (not under the catalyst reduction conditions). Thus, the results presented in tables are directly related to the effect of structural catalyst modifications occurring during their operation. In this way, relative content of Pt and Co components with high valency (II or IV) indicates the atoms which were on the metallic nanoparticles surface or in dissolved species (not yet reduced) distributed in the catalytic layer volume.

In PtCo/C material after catalytic layer preparation and 4-h conditioning (a crucial process for obtaining a suitable initial cell performance) performed in fuel cell at 70 °C and 0.6 V (0-PtCo/C) the XPS atomic ratio changed to 3.7:1 indicating a reduction of Pt relative content in particle external shell. Simultaneously, XRD Pt:Co atomic ratio increased to 3.5:1 indicating this time a

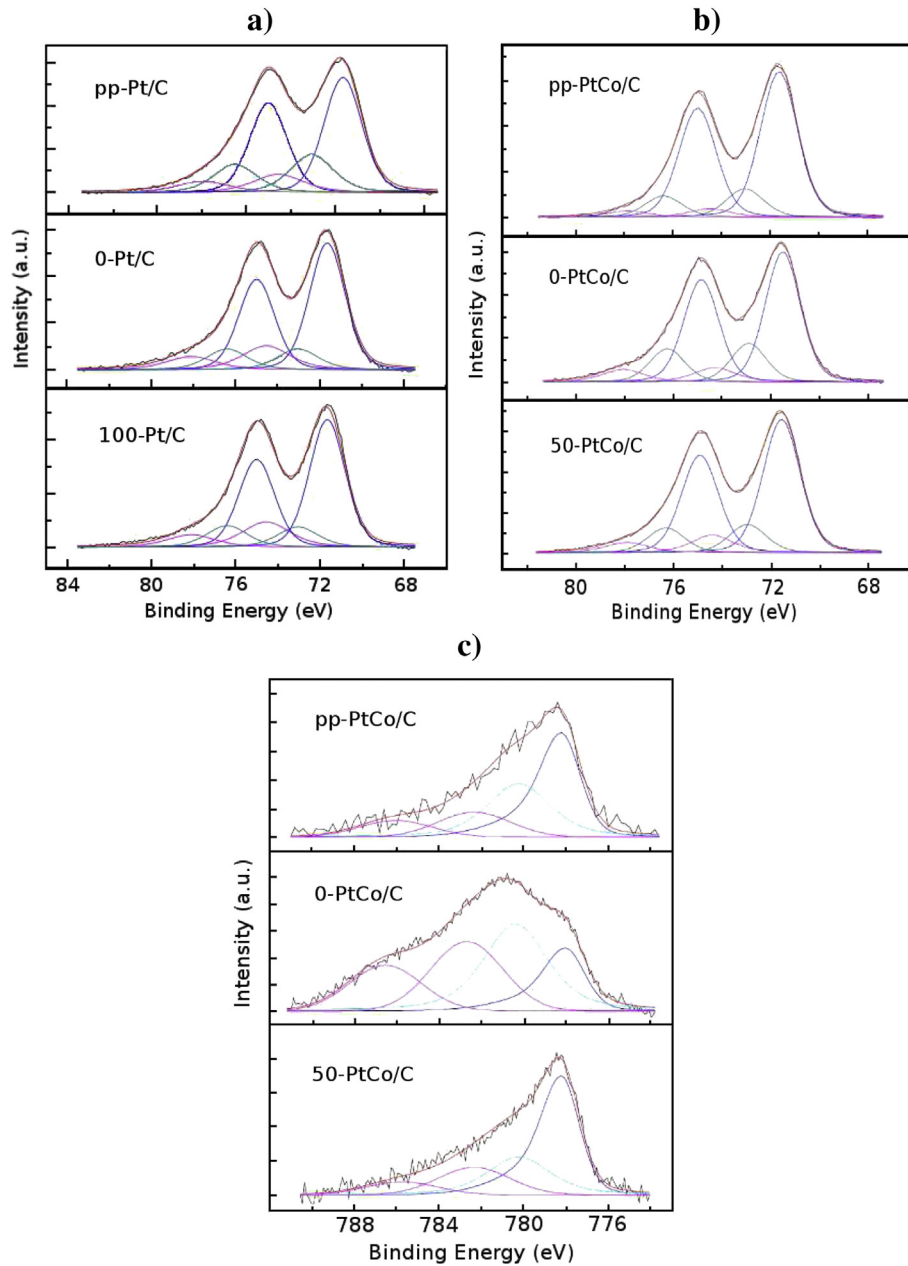


Fig. 3. The XPS spectra fitting results of considered electrocatalysts in the form of pristine powder (pp-Pt/C, pp-PtCo/C), as prepared electrode (0-Pt/C, 0-PtCo/C) and worked electrode (only 100-Pt/C and 50-PtCo/C are shown as the others are very similar). a-b) Pt(4f_{7/2}) and Pt(4f_{5/2}) spectrum: blue peaks correspond to metallic state Pt⁰; light blue – to Pt^{II}; pink – to Pt^{IV}. c) Co(2p_{3/2}) spectrum: blue peaks correspond to metallic state Co⁰; light blue – to Co^{II}; pink – to two shake-up satellite peaks of Co^{II} [28]. (For interpretation of the references to colour in this figure legend, the reader is referred to the web version of this article.)

reduction of Co relative content in particle core. XAS-determined value remained unchanged. During our previous *in situ* XAS study [19] it was observed that in the case of MEA composed of PtCo/C cathode catalyst conditioning process also resulted in the local structure modification in metallic nanoparticles. The main changes in the XAS signals were interpreted as a result of cobalt dissolution (Co bonded to O and not fully alloyed with Pt), correlated with a slight increase in chemical disorder on the particle surface and increase in local structural order in the particle core. Now, taking into account XPS data, possible scenario of modifications occurring during MEA activation can be expanded as follow (considering also other results presented in Table 1 and in Ref. [19]): during the catalyst preparation stage, Co atoms from the interior of

the nanoparticles migrated to their surface [31], and/or small particles composed predominantly from cobalt atoms dissolved, diffused in the ionomer phase and precipitated on the surface of bigger ones. This agrees with previous TEM analysis from which resulted that particles smaller than 3 nm almost disappeared during this stage of catalyst work and particles size distribution asymmetry decreased indicating a possible occurrence of Ostwald ripening process. As a result, core of the nanoparticle reached a mean stoichiometry Pt_{3.5}Co (XRD-determined Pt/Co value, Table 1) and became more ordered (previous XAS analysis results, [19]), while the surface of the nanoparticle exhibited lower Pt relative content with respect to pristine powder (mean Pt:Co ratio reached at least 4:1 assuming this time 0.25 nm thick surface shell, cf. D_{ave} in

Table 2

Relative amounts of Pt atoms in metallic state, $\text{Pt(OH)}_2/\text{PtO}$ and PtO_2 determined by fitting the Pt(4f) XPS spectra.

Sample	Pt^0 (%)	Pt^{II} (%)	Pt^{IV} (%)
pp-PtCo/C	78(2)	17(2)	5(2)
0-PtCo/C	69(2)	20(2)	12(2)
50-PtCo/C	68(2)	20(2)	12(2)
100-PtCo/C	66(2)	22(2)	12(2)
150-PtCo/C	67(2)	20(2)	13(2)
pp-Pt/C	62(2)	25(2)	13(2)
0-Pt/C	69(2)	14(2)	17(2)
100-Pt/C	66(2)	16(2)	18(2)
150-Pt/C	66(2)	16(2)	18(2)

Table 1) and became chemically slightly less ordered (*cf.* chemical order parameter in **Table 1**). Schematic representation of nanoparticle structure is shown in **Fig. 4**. Furthermore, dissolved Co species were still present and rather homogeneously distributed in the catalytic layer (*cf.* XAS-extracted Pt/Co ratios in **Table 1**).

In the worked PtCo/C electrocatalyst (50-, 100- and 150-PtCo/C) the relative amount of Co atoms as viewed by XPS decreased gradually in time (Co:Pt dropped down to 1:5). Moreover, it should be noted that the biggest change was observed after first 50 h of work and that particle core composition after this time reached Pt_4Co stoichiometric relation (*cf.* XRD-determined Pt/Co ratio, **Table 1**). Taking also into account high stability of the particle size distribution and increasing chemical and structural order (especially in Pt–Co two-body distribution, [19] and **Table 1**) it can be concluded that during this stage of catalyst work under step-like potential cycling (first 50 h), segregation of Co atoms at the surface of the particle progressed. Co atoms belonging to the

nanostructure surface and those not fully alloyed with platinum were intensively dissolved and finally removed from the catalytic layer. As a consequence, a core–shell nanoparticle structure with Pt-rich and very thin shell started to be formed (**Fig. 4**). Subsequent hours of electrocatalyst work in a fuel cell resulted in a progressive Co depletion in particles surface, especially in the catalytic layer region close to cathode/membrane interface (compare XPS-extracted Pt/Co values with XRD and XAS ones, **Table 1**). Finally (after 150 h), Pt/Co atomic ratio on the particles surface reached value decisively higher than 5.0. Since external particles shell was thinner than 0.25 nm, we assumed a possible Pt-skin formation (**Fig. 4**). In these stages the Co atoms migration from particles interior to the surface was almost stopped (nanoparticle core stoichiometry remained stable, *cf.* XRD-determined Pt/Co ratios in **Table 1**). Co dissolution slowed down, but dissolved cobalt species still present in the ionomer phase were systematically removed from superficial part of the catalytic layer (*cf.* XPS and XAS-determined stoichiometries in **Table 1**) and diffused to the polymer membrane where they were probably accumulated, as was shown in Ref. [30].

Lets look now at the estimated relative valency of Pt and Co components present on the external shell of nanoparticles in PtCo/C electrocatalyst in subsequent degradation stages (see **Tables 2** and **3**, respectively). Starting from the first one, conditioning lasting 4 h, we just know that after this period outer shell of particles and their surface became Co richer (*cf.* **Fig. 4**) and more disordered but many dissolved species were still present in catalytic layer (4-h conditioning was probably too short to remove all impurities and oxides from catalyst material [19]). As a consequence relative contents of Pt^{II} , Pt^{IV} and Co^{II} were higher than in pristine powder (**Tables 2** and **3**, respectively). Calculations performed on the basis of the nanoparticle structural model constructed for 0-PtCo/C combining XRD/TEM/XAFS and XPS data (**Fig. 4**) showed that the amount of oxidized platinum corresponds to the amount of Pt atoms belonging to the nanoparticles surface. Whereas, the relative contribution of Co^{II} was at least two times higher than the surface Co contribution as calculated from the nanoparticle structural model. To reproduce XPS amount of Co^{II} it should be assumed that after PtCo/C catalyst conditioning in the catalytic layer close to the membrane/cathode interface a predominant part of the dissolved species accounted for oxidized cobalt (in agreement with observations presented in the first part of this discussion).

Table 3

Relative amounts of Co atoms in metallic state and CoO determined by fitting the $\text{Co}(2\text{p}_{3/2})$ XPS spectra.

Sample	Co^0 (%)	Co^{II} (%)
pp-PtCo/C	62(2)	38(2)
0-PtCo/C	37(2)	63(2)
50-PtCo/C	70(2)	30(2)
100-PtCo/C	66(2)	34(2)
150-PtCo/C	67(2)	33(2)

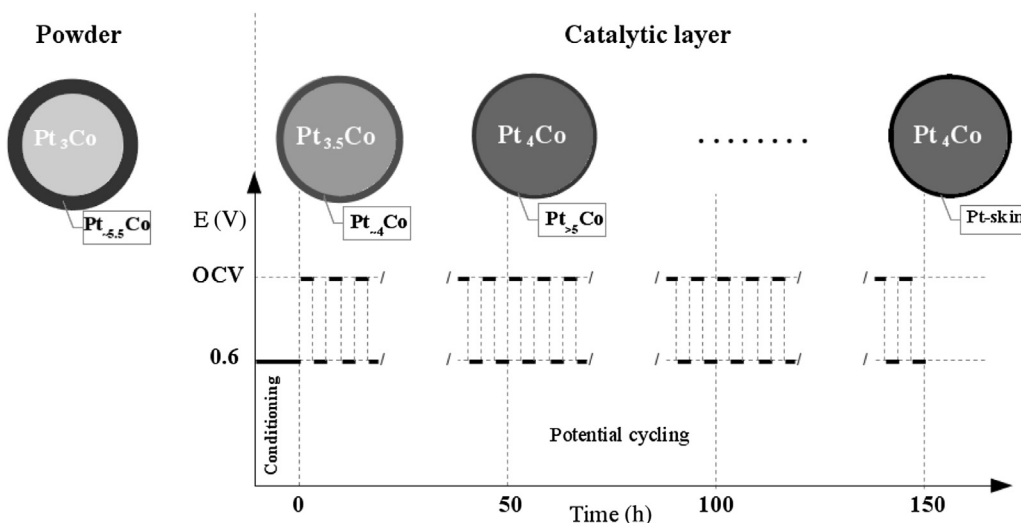


Fig. 4. Schematic representation of modifications observed in the structure of Pt–Co nanoparticles in 30%PtCo/Vulcan electrocatalyst on each studied operation stage as resulted from combined XPS and XRD/TEM analysis.

After 50 h of work under potential cycling conditions, the relative amount of oxidized Co components in PtCo/C electrocatalyst decreased severely resulting in $\text{Co}^{II}/\text{Co}^0$ ratio drop from 1.7 to 0.4, and remained quite unchanged during the subsequent 100 h. Such a result confirmed an intensive removal of dissolved Co species from XPS sensitive region of catalytic layer occurring mainly during the first several hours of potential cycling. On the contrary, relative content of Pt^{II} and Pt^{IV} remained unchanged over the whole 150 h of catalyst work corroborating the idea that negligible part of platinum atoms was subjected to the dissolution process. XAS data analysis [19] showed exactly the same trend of changes: strong increase of Co oxidation level after catalytic layer preparation and then after 50 h of step-like potential cycling even stronger decrease in Co–O contribution (almost reaching the limit of XAS measurement sensitivity). Moreover, XAS results indicated that Co sites were involved in structural modifications and mainly during the first hours of FC operation, while local neighborhood of Pt atoms exhibited high structural stability. It is worth to mention that PtO_x contribution to total XAS signal for each sampled electrode was below the measurement sensitivity. Using all these data and results of calculations [11] showing that Co in the subsurface rather than on the exposed surface enhances the stability of Pt atoms, we can suppose that in considered PtCo/C catalytic material Pt-skin structure started to be formed just after the first cycling hours and then only progressive skin ordering occurred. These modifications in the nanoparticle surface are clearly correlated with the electrochemical performance of the fuel cell. In other words, until the Pt-skin structure started to be visible (after the first 50 h of cycling) a mild loss of cathode catalyst activity was observed (from 0-PtCo/C to 50-PtCo/C current density at 0.8 V decreased over 30 mA cm^{-2} , Fig. 1), then only progressive skin ordering occurred and was accompanied by progressive slight increase of this activity (from 50-PtCo/C to 150-PtCo/C current density at 0.8 V increased of about 25 mA cm^{-2} , Fig. 1).

4.3. Degraded Pt/C electrocatalyst

In the case of Pt/C material forming a cathode catalytic layer a clear reduction in the relative amount of platinum oxides in 0-Pt/C with respect to pp-Pt/C was noted (Table 2). Effect was strong enough to be also visible in XAS spectra [21]. For XPS measurements, this change may be reasonably attributed to the modifications in metallic granular structure (increase of particle size distribution asymmetry on the large-sized particle side) and to complete activation of Pt/C catalyst by 4-h conditioning at 70 °C and 0.6 V. This means, that during this relatively short period a major component of soluble oxidized Pt species diffusing in the ionomer phase, probably mainly toward the membrane, precipitated on the other particles and/or migrated to the polymer membrane leaving the catalytic layer. Thus, these large-sized particles (from the tail of the size distribution) were located mainly in the XPS sampled region (volume-to-surface atom ratio increase means $(\text{Pt}^0):(\text{Pt}^{II} + \text{Pt}^{IV})$ ratio increase).

Regarding Pt/C catalyst working under step-like potential cycling conditions, relative amounts of Pt^{II} and Pt^{IV} remained unchanged over whole 150 h of accelerated degradation, as in PtCo/C catalyst. However, in this case pure Pt metallic granular structure of electrocatalyst continuously varied during FC operation ([22] and Table 1). The mean nanoparticle size from stage to stage systematically increased (at the beginning mainly through the dissolution/precipitation process and later by particles agglomeration and coalescence). Obviously, this had to be followed by systematical increase in volume-to-surface atom ratio: from 1.0 to 1.4 for particles with mean size 2.4 nm and 3.1 nm, respectively. Instead, XPS extracted data showed this ratio quite constant and equaled to

about 2.0 (this ratio corresponds to the mean particle size larger than 4.0 nm). Taking into consideration processes occurred during conditioning and that particle size distribution became more asymmetric with working time, reaching for long-operated catalyst even bimodal shape with a mean diameter of large-sized part of over 6 nm (cf. Table 1), it can be concluded that as a result of potential cycling large particles were formed mainly in the XPS sampled region, i.e. near to cathode/membrane interface (in agreement with data presented in Ref. [29]).

5. Conclusions

In the present contribution, XPS spectra analysis performed for a set of carbon supported Pt and Pt–Co catalysts, subjected to accelerated degradation in a real fuel cell, were presented. Results were discussed in the light of previously published data of TEM, XRD and XAS measurements. It should be underlined that the dynamics of structural modifications observed in the nanoparticles surface region (i.e. working-time dependent variations) is compatible with changes observed by XRD and XAS techniques. Combining all the methods, exhibiting different sensitivity to physical parameters, it was possible to construct a detailed model of the catalyst atomic structure, with the quantitative determination of the nanoparticle surface composition. We were able to extract some information regarding the catalysts degradation mechanisms on each considered stage of catalyst operation: starting from the pristine powder, through the conditioned electrode, to electrodes operating in fuel cells under step-like potential cycling conditions.

The obtained results confirmed strong potential cycling-induced structural modifications in both electrocatalysts. However, for Pt/C catalyst these changes were a consequence of working conditions stimulating intensive solubility of oxidized Pt and their precipitation leading to a systematic growth of the mean nanoparticle size. Moreover, it was noted that the large particles were formed mainly in the region close to the cathode/membrane interface. In the case of PtCo/C catalyst the biggest structural modifications were associated with the atomic level changes in which cobalt atoms were mainly involved. It was also demonstrated that alloying platinum with cobalt led to lowering their solubility and to the formation (under FC operation conditions) of Pt–Co nanoparticles with structure composed of a stable Pt_4Co alloy core covered by thin Pt-rich shell and finally by Pt-skin which exhibited higher structural stability than nanoparticles composed of only Pt. Additionally, it was observed that slight variations in PtCo/C cathode catalyst activity during FC operation under step-like potential cycling are strongly correlated with structural modifications occurred in the thin external shell of Pt–Co nanoparticles.

Acknowledgments

We gratefully acknowledge the invaluable help from Dr Sonia Dsoke and Prof. Roberto Marassi from Chemistry Department at University of Camerino during electrodes preparation and degradation.

References

- [1] G. Hoogers, D. Thomsett, Catal. Technol. 3 (1999) 106.
- [2] N.M. Markovic, P.N. Ross Jr., Catal. Technol. 4 (2000) 110–126.
- [3] M.S. Dresselhaus, I.L. Thomas, Nature 414 (2001) 332–337.
- [4] L. Schlapbach, A. Zuttel, Nature 414 (2001) 353–358.
- [5] B.C.H. Steele, A. Heinzel, Nature 414 (2001) 345–352.
- [6] N.M. Markovic, P.N. Ross, Surf. Sci. Rep. 45 (2002) 117–230.
- [7] W. Vielstich, A. Lamm, H.A. Gasteiger, Handbook of Fuel Cells, Fundamentals Technology and Applications, Wiley, West Sussex, 2003.
- [8] K. Kinoshita, Electrochemical Oxygen Technology, Wiley, New York, 1992.

- [9] E. Antolini, J.R.C. Salgado, E.R. Gonzalez, *J. Power Sources* 160 (2006) 957–968.
- [10] V.R. Stamenkovic, B. Fowler, B.S. Mun, G.F. Wang, P.N. Ross, C.A. Lucas, N.M. Markovic, *Science* 315 (2007) 493.
- [11] Y. Ma, P.B. Balbuena, *J. Phys. Chem. C* 112 (2008) 14520–14528.
- [12] J. Greeley, I.E.L. Stephens, A.S. Bondarenko, T.P. Johansson, H.A. Hansen, T.F. Jaramillo, J. Rossmeisl, I. Chorkendorff, J.K. Norskov, *Nat. Chem.* 1 (2009) 552–556.
- [13] S. Chen, H.A. Gasteiger, K. Hayakawa, T. Tada, Y. Shao-Horn, *J. Electrochem. Soc.* 157 (2010) A82–A97.
- [14] E. Antolini, J.R.C. Salgado, M.J. Giz, E.R. Gonzalez, *Int. J. Hydrogen Energy* 30 (2005) 1213–1220.
- [15] P. Yu, M. Pemberton, P. Plasse, *J. Power Sources* 144 (2005) 11–20.
- [16] H.A. Gasteiger, S.S. Kocha, B. Sompalli, F.T. Wagner, *Appl. Catal. B* 56 (2005) 9.
- [17] V.R. Stamenkovic, B.S. Mun, M. Arenz, K.J.J. Mayrhofer, ChA. Lucas, G. Wang, P.N. Ross, N.M. Markovic, *Nat. Mater.* 6 (2007) 241–247.
- [18] G. Greco, A. Witkowska, E. Principi, M. Minicucci, A. Di Cicco, *Phys. Rev. B* 83 (2011) 134103.
- [19] G. Greco, A. Witkowska, M. Minicucci, L. Olivi, E. Principi, S. Dsoke, A. Moretti, R. Marassi, A. Di Cicco, *J. Phys. Chem. C* 116 (2012) 12791–12802.
- [20] A. Witkowska, A. Di Cicco, E. Principi, *Phys. Rev. B* 76 (2007) 104110.
- [21] A. Witkowska, E. Principi, A. Di Cicco, S. Dsoke, R. Marassi, L. Olivi, M. Centazzo, V. Rossi Albertini, *J. Non-Cryst. Solids* 354 (2008) 4227–4232.
- [22] A. Witkowska, G. Greco, S. Dsoke, R. Marassi, A. Di Cicco, *J. Non-Cryst. Solids* 401 (2014) 169–174.
- [23] J.F. Moulder, W.F. Stickle, P.E. Sobol, K.D. Bomben, *Handbook of X-Ray Photoelectron Spectroscopy*, Physical Electronic Inc, 2005.
- [24] D.A. Shirley, *Phys. Rev. B* 5 (1972) 4709.
- [25] M. Aronniemi, J. Sainio, J. Lahtinen, *Surf. Sci.* 578 (2005) 108–123.
- [26] P. Stonehart, *Phys. Chem.* 94 (1990) 913–921.
- [27] Y. Lu, R.G. Reddy, *Electrochim. Acta* 52 (2007) 2562–2567.
- [28] N.S. McIntyre, M.G. Cook, *Anal. Chem.* 47 (1975) 2208–2213.
- [29] P.J. Ferreira, G.J. la O', Y. Shao-Horn, D. Morgan, R. Makharla, S. Kocha, H.A. Gasteiger, *J. Electrochem. Soc.* 152 (2005) A2256–A2271.
- [30] A. Seo, J. Lee, K. Han, H. Kim, *Electrochim. Acta* 52 (2006) 1603–1611.
- [31] L. Dubau, J. Durst, F. Maillard, L. Guetaz, M. Chatenet, J. Andre, E. Rossinot, *Electrochim. Acta* 56 (2011) 10658–10667.